Very-low-temperature electrical resistivity of *K*Rb, *K*Na, and *Li*Mg alloys

J. Zhao,* Y. J. Qian, Z.-Z. Yu,† M. L. Haerle,‡ S. Yin,§ H. Sato,**
W. P. Pratt, Jr., P. A. Schroeder, and J. Bass
Department of Physics and Astronomy, Michigan State University, East Lansing, Michigan 48824-1116
(Received 8 July 1988; revised manuscript received 21 July 1989)

Previous high-precision measurements below 0.5 K showing a resistivity anomaly in *K*Rb and dilute *K*Na and *Li*Mg alloys have been extended to *K*Na and *Li*Mg alloy samples which cover the residual-resistivity range from $\rho_0 = 4\times10^{-10}$ to 1.7×10^{-7} Ω m. Residual-resistivity data per atomic percent impurity are consistent for all three alloys with literature results in the regions of overlap. The data for all three alloys also show the expected behavior for inelastic electron-impurity scattering. At temperatures above 1 K, the *K*Rb and *K*Na alloy data show increases in electron-phonon scattering with increasing ρ_0 probably due to quenching of phonon drag and—for *K*Rb—to reduction in the Debye temperatures of the alloys. All three alloy systems display a low-temperature anomaly which has a universal magnitude for a given ρ_0 when $\rho_0 < 10^{-7}$ Ω m, and which varies approximately linearly with both temperature and residual resistivity. Localization, electron-electron interaction, and Kondo effects appear to be ruled out as explanations for the anomaly in this regime. Published models based on charge-density waves and ineffectiveness of electron-phonon scattering are also considered. As ρ_0 increases above 10^{-7} Ω m, the anomalous behavior approaches the electron-electron interaction limit. In the very-high-concentration *Li*Mg alloys microscopic differences between the alloys are found to affect the data.

I. INTRODUCTION

We recently briefly reported[1] an unexpected resistivity anomaly in *K*Rb alloys and dilute *K*Na and *Li*Mg alloys. We argued that this anomaly was not due to a Kondo effect[2] (because it was not affected by application of a magnetic field and it had no associated thermoelectric anomaly) or to localization and interaction effects[3] (because it was too large for both effects and increased much more slowly with increasing residual resistivity ρ_0 than either effect). In order to further our understanding of this anomaly, we have now extended measurements to more concentrated *K*Na and *Li*Mg alloys. These new measurements extend up to values of ρ_0 large enough that interaction effects should become visible. In this paper, we describe both our old and new measurements, and discuss possible interpretations of what we see. Of particular interest experimentally are whether the form and magnitude of the anomaly are the same for *K*Rb, *K*Na, and *Li*Mg and where the transition from this anomaly to interaction effects occurs.

The paper is organized as follows. In Sec. II we describe sample preparation procedures and our measurement technique. In Sec. III we briefly review the standard theory of the low-temperature resistivity of simple metals, along with published models of the resistivity of dilute alloys that might be expected to be relevant to our data. In Sec. IV we present our experimental data and compare them with the predictions of these models. Section V contains a summary and conclusions.

Concurrently with our measurements of electrical resistivity, we also always measure the thermoelectric ratio G of our samples. At low temperatures, where the Sommerfeld value of the Lorenz ratio is attained, the two transport coefficients ρ and G completely specify the electronic transport behavior of cubic metals such as K and Li. So as not to complicate the presentation of our results, we will describe the G data in a separate paper.[4]

II. SAMPLE PREPARATION AND EXPERIMENTAL TECHNIQUE

The samples were fabricated from 99.95% pure K, Rb and Na obtained from Callery Chemical Division of Mine Safety, Inc., and 99.99% pure Li obtained from Atomergic Chemetals Corporation. All the samples in this study were wires prepared by extrusion from stainless-steel presses through stainless-steel dies. K, Rb, and Na melt not far above room temperature. Inside an Ar-filled glove box, the alloy constituents for the *K*Rb and *K*Na alloys were weighed out, melted, and mixed together on a glass container on a hot plate. The liquid alloys were poured into the stainless-steel presses. Because of the high melting point of Mg, an initial master *Li*(1 at. % Mg) alloy—all alloy concentrations in this paper are given in atomic percent—was made inside a stainless-steel crucible under Ar atmosphere in an induction furnace and then diluted to make less concentrated alloys by adding Li and melting the mixture on a hot plate inside the glove box. We later found that just mixing Mg carefully into molten Li in a stainless crucible on a hot plate inside the glove box also gave satisfactory alloys, and this procedure was used for *Li*(1 at. % Mg), *Li*(10 at. % Mg), *Li*(20 at. % Mg), and *Li*(32 at. % Mg) alloys. The two *Li*(1 at. % Mg) alloys prepared in different ways gave the same results in all the measurements. A *Li*(49 at. % Mg)

sample was made in the induction furnace. The *Li*(32 at. % Mg) and *Li*(49 at. % Mg) samples were annealed at 70% of their melting temperatures under vacuum for about two days to attempt to equilibrate the impurity distribution.

The samples were mounted in a sample can, sealed, and transferred to a dilution refrigerator. All samples were bare, free-hanging, and generally had shiny surfaces both before and after the measurements.

The measurements were four-probe. Most of the potential leads were made of the same material as the samples and simply stuck onto the samples. For *Li*Mg samples with Mg concentrations higher than 10 at. %, the alloys were hard and unsticky, so that potential leads made from the same alloys had to be fused onto the samples with a clean soldering iron inside the glove box. For *Li*Mg alloys with Mg concentrations of 32 at. % and above, this method sometimes gave unusual $d\rho/dT$ and G behavior which we presume was due either to metals from the soldering iron tip diffusing into the samples or to formation of unwanted compounds during the relatively high-temperature fusing. We later developed a cold welding technique that used pure K as the low-temperature thermal and electrical connector for these high-concentration alloys. K is essentially insoluble in Li, Mg, and Cu, and is sticky at room temperature, which makes it easy to cold weld onto samples and copper connectors. With this technique we found no unusual behavior.

In the alloy systems we studied, the ratio of the temperature-dependent resistivity to the residual resistivity $\rho(T)/\rho_0$ ranged from 10^{-4} to 10^{-6}. Thus, to measure the resistivity change as a function of temperature with 1% accuracy, it was necessary to resolve resistance to parts in 10^6–10^8. Furthermore, the resistances of our samples were in the range 10^{-6}–10^{-4} Ω, and to avoid self-magnetoresistance and heating, the current passing through the sample had to be kept as small as possible. For a current of 100 mA, it is necesssary to detect a signal as small as 10^{-15} V to achieve the necessary high resolution. We achieved voltage sensitivities of 10^{-15} V (limited only by Johnson noise) and precisions of a few parts in 10^8 by using a superconducting quantum interference device (SQUID) null detector in conjunction with a current comparator.[5] A detailed description of our measuring techniques and procedures is given elsewhere.[5] We note here only that we were able to improve our previous precision from one part in 10^7 to about two parts in 10^8 by using a programmable digital voltmeter to average the out-of-balance signal beyond the last dial of the current comparator.

The quantity measured with the current comparator was the ratio c of the resistance of the sample of interest to that of another—usually nearly identical—sample, which we call the reference resistor. The reference resistor was held at a fixed temperature T, and the ratio was measured with the sample held first at T and then at $T+\Delta T$. T and ΔT were also measured, allowing us to calculate the quantity

$$[c(T+\Delta T)-c(T)]/c\,\Delta T\ . \tag{1}$$

It is straightforward to show[5] that this quantity closely approximates $(1/\rho)(d\rho/dT)$ evaluated at $T+(\Delta T/2)$. $\Delta T/T$ ranges from 0.06 to 0.4 with an average of 0.2. Below 1 K, ρ is just the residual resistivity ρ_0, so that by multiplying Eq. (1) by ρ_0, we obtain $d\rho/dT$. This is one of the quantities we plot. Alternatively, we can divide $d\rho/dT$ by the average temperature $T+(\Delta T/2)$ to get $(1/T)(d\rho/dT)$. A plot of this latter quantity is useful for investigating deviations from the standard T^2 behavior (see Sec. III), since a T^2 variation would give a horizontal straight line.

III. THEORY

A. The standard model

The standard model of low-temperature resistivity in a dilute alloy contains four elements:[6,7] elastic electron-impurity scattering, electron-electron scattering, inelastic electron-impurity scattering, and electron-phonon scattering. This model predicts a resistivity of the form

$$\rho(T)=\rho_0+AT^2+B\rho_0T^2+MT^5+N\exp-(T/\Theta^*)\ . \tag{2}$$

The residual resistivity ρ_0 is due to the lowest-order term in elastic impurity scattering. A term of the form AT^2 is expected on very general grounds[2] from electron-electron scattering. The term $B\rho_0T^2$ arises from a competition[7] between inelastic electron-impurity scattering which gives a term $2B\rho_0T^2$, and higher-order elastic electron-impurity scattering which gives $-B\rho_0T^2$. Finally, at low temperatures in the alkali metals, normal and Umklapp electron-phonon scattering would be expected to give rise to T^5 and exponential terms, respectively.[6] Experimentally, the electron-phonon resistivity in pure K has been found to vary exponentially with temperature[9,10] down to about 1 K. This behavior can be explained on the basis that the T^5 term is eliminating by phonon drag.[10,11]

In high-purity K or Li below 1 K, the electron-phonon terms MT (Ref. 5) and $N\exp(-T/\Theta^*)$ are negligibly small.[10,12] In such a case, the standard model would predict a simple T^2 dependence for ρ:

$$\rho=\rho_0+(A+B\rho_0)T^2\ . \tag{3}$$

Since we are interested primarily in the temperature-dependent portion of the resistivity $\rho(T)$, we can eliminate ρ_0 by taking the temperature derivative of ρ which, from Eq. (3) would be

$$d\rho/dT=2(A+B\rho_0)T \tag{4a}$$

or, if we divide by the temperature T,

$$(1/T)(d\rho/dT)=2(A+B\rho_0)\ . \tag{4b}$$

We see from these two equations that if we plot $d\rho/dT$ versus T we would expect to find a straight line passing through the origin, and if we plot $(1/T)(d\rho/dT)$ versus T we would expect to find a horizontal straight line. Both types of plot will be used in this paper.

Figure 1 shows the forms of $(1/T)(d\rho/dT)$ for high-

purity alkali metals from 0.1 to 2.5 K. We see that the data for Li are flat above about 1.5 K (and they remain flat till well above 4 K).[13] The data for Na are almost flat from 1 to 3 K, and the data for K are flat between 0.3 and 1.2 K. In contrast, the data for Rb are not flat anywhere in the temperature range. Noting that the Debye temperatures for these metals decrease in the order $\theta_D(\mathrm{Li}) > \theta_D(\mathrm{Na}) > \theta_D(\mathrm{K}) > \theta_D(\mathrm{Rb})$, we attribute the upturns at temperatures above the flat regions to the onset of electron-phonon scattering as described in Eq. (2). The upturns below the flat regions are sample dependent and probably associated with scattering by residual dislocations in the samples.[14] The absence of a flat region in Rb is ascribed to domination of the high- and low-temperature upturns over the T^2 contribution at all temperatures.

B. Beyond the standard model

As we shall describe later, a very general anomalous low-temperature behavior which deviates from Eq. (3) develops as the alloy concentrations increase in *K*Rb, *K*Na, and *Li*Mg alloys. If we ask what might cause such deviations from the standard model in dilute alkali metal alloys, five possibilities immediately arise: (i) a Kondo effect;[2] (ii) two-level systems due to the presence of impurities;[15] (iii) effects of a possible charge-density-wave (CDW) ground state in the alkali metals;[16] (iv) a recently proposed ineffectiveness condition for electron-phonon scattering at low temperature;[17] and (v) quantum localization and interaction due to the disorder introduced by the impurities.[3] We consider each of these in turn.

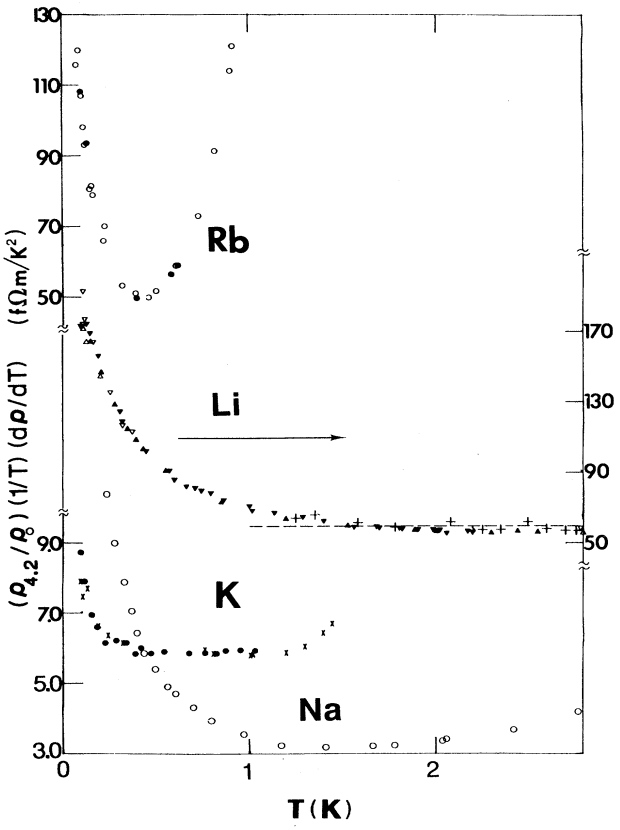

FIG. 1. $(\rho_{4.2\,\mathrm{K}}/\rho_0)(1/T)(d\rho/dT)$ vs T for pure Rb, Li, K, and Na. $R(295\ \mathrm{K})/R(1\ \mathrm{K})$ has the approximate values: 400 for Rb, 1000 for Li, 5800 for K, and 4700 for Na.

1. *Kondo effect*

The Kondo effect, associated with the flipping of electrons spin during scattering from an isolated magnetic impurity, gives rise to a resistivity anomaly qualitatively similar to the one we see. The resistivity component arising from the Kondo effect should have the form[2]

$$\rho(T) \propto c\left[1+\frac{J}{E_F}\ln\left[\frac{k_B T}{E_F}\right]\right], \tag{5}$$

where c is the impurity concentration, k_B is Boltzmann's constant, E_F is the Fermi energy, and J is the spin coupling constant. This effect is expected to have a strong magnetic field dependence and also to be accompanied by a thermoelectric anomaly.

2. *Two-level systems*

Another possible source of anomalous resistivity is a two-level system which was invoked for a while to explain resistivity anomalies in disordered systems such as metallic glasses.[15] If the ground state of the disordered systems has a nearby excited state, separated from the ground state by a subtle difference in spatial ordering, then there is expected to be a contribution to $\rho(T)$ of the form[15]

$$\rho \propto \ln[k_B^2(T^2+T_0^2)] . \tag{6}$$

If such a two-level system arises from the host configuration in the vicinity of a single impurity, or from a nonsymmetric impurity location in the host, the contribution to $\rho(T)$ would be proportional to ρ_0. If it requires an interaction between two impurities, the contribution would be proportional to ρ_0^2.

3. *Charge-density-wave related effects*

Overhauser[16] has argued vigorously that the ground state of the alkali metals is a CDW state, and that phason excitations from this ground state play an important role in describing various physical properties, including transport properties. Very recently, Hu and Overhauser have proposed[18] that the vertex correction to the electron-phason interaction, combined with the presence of a Fermi surface having two distinct groups of electrons, can give rise to an anomaly similar to the one we see in *K*Rb alloys. They solved the Boltzmann transport equation for a Fermi surface consisting mostly of a sphere, but with small cylindrical surfaces located between the main CDW gap and the first minigap. Electrons near the cylindrical parts of the surface were taken to be affected by electron-phason interactions, while electrons near the spherical parts were taken to be unaffected. Assuming an isotropic

CDW Q-domain distribution, and choosing parameters determined from CDW-based fits to other data, they were above to provide reasonable fits to our data for 9.4 at. % KRb and 23.6 at. % KRb from 1.8 K down to 0.2 K.[18]

4. *Ineffectiveness condition for electron-phonon scattering*

Recently Kaveh and Wiser[17] suggested that the Koshino-Taylor[7] theory of inelastic electron-impurity scattering should be modified based on the Pippard ineffectiveness condition that long wavelength phonons are ineffective in scattering electrons for which the elastic electron mean free path l is shorter than the phonon wavelength. They proposed that there should be a cutoff at $q_{\min}=\pi/l$ in the integral over all phonon states q, which causes the inelastic electron-impurity scattering term $(+2B\rho_0T^2)$ to gradually disappear as the temperature decreases, leaving only the higher-order elastic term $(-B\rho_0T^2)$ at sufficiently low temperatures. Using the Debye approximation for the phonon density of states, they reported that their modification of the Koshino-Taylor term gave an excellent fit to the low-temperature anomalous resistivities of KRb alloys down to the lowest temperatures reached in our experiments (≈ 0.1 K), and noted that still lower-temperature measurements could provide a definite test for this model. Unfortunately, still lower-temperature measurements require greater precision (parts in 10^9) than we currently have available (parts in 10^8).

5. *Weak localization and interaction*

In the past few years there has been a growing realization that disordered materials cannot be understood by forcing them into the mold of ordered systems. As the electron mean free path becomes short, quantum corrections to the Boltzmann transport theory can no longer be neglected. Our samples are in the weak-localization regime (WLR), i.e., $(k_Fl)^{-1}\ll 1$, where k_F is the Fermi wave vector. In the WLR there is interference between scattered partial waves, which can be significant in very short mean-free-path samples. There are two aspects of corrections: the localization effect, which involves quantum interference, and the interaction effect, which involves modification of the electron-electron interaction.

The correction to the traditional conductivity of three dimensional systems due to localization has been calculated to have the form[3]

$$\Delta\sigma_{\rm lo}(T)=\frac{e^2}{\hbar\pi^2}\frac{1}{L_{\rm th}} , \tag{7}$$

where $L_{\rm th}=(D\tau_{\rm in})^{1/2}$, $\hbar$ is Planck's constant divided by 2π, $\tau_{\rm in}$ is the inelastic relaxation time, and D is related to the conductivity by the Einstein relation $\sigma=D(e^2/\hbar)(dn/d\epsilon)_{\epsilon_F}$, where n is the electron density.

The interaction between electrons in the presence of a random potential in three-dimensional systems has been predicted to give the following addition to the conductivity:[3]

$$\Delta\sigma_{\rm in}=\frac{e^2}{\hbar}\frac{1}{4\pi^3}\frac{1.3}{\sqrt{2}}\left(\tfrac{4}{3}-\tfrac{3}{2}\tilde{\tilde{F}}\right)\sqrt{k_bT/\hbar D} . \tag{8}$$

Here k_b is Boltzmann's constant

$$\tilde{\tilde{F}}=\tfrac{32}{3}[1+3F/4-(1+F/2)^{3/2}]F ,$$

$F(x)=(1/x)\ln(x+1)$, $x=(2k_F/k_0)^2$, and k_F and k_0 are, respectively, the Fermi wave vector and the Thomas-Fermi screening vector.

If we assume that $\rho(T)$ in Eq. (3) is dominated by inelastic electron-impurity scattering,[8] then for our values of ρ_0, Eqs. (7) and (8) predict that the interaction term should predominate over the localization term, and produce a $(1/T)d\rho/dT$ that varies as $T^{-3/2}\rho_0^{5/2}$. The coefficients of the interaction term can be calculated from Eq. (8), which is a function only of the electron density, and then only weakly. A rigid band estimate of the correction to the magnitude of Eq. (8) due to alloying of Li with divalent Mg yields less than 10% change for 32 at. % Mg. Thus, we can use free-electron values of k_F for the solvent metals to evaluate Eq. (8) for the alloys.

IV. EXPERIMENTAL RESULTS AND ANALYSIS

We assume that the resistivities of these alloy systems can be described as

$$\rho=\rho_0+f(\rho_0,T)+AT^2+B\rho_0T^2+g(\rho_0,T) , \tag{9}$$

where f is a low-temperature anomalous contribution to ρ and g is a high-temperature term which only becomes significant for $T>1.2$ K. The quantity we studied can be expressed as

$$\frac{1}{T}\frac{d\rho}{dT}=\frac{f'}{T}+2A+2B\rho_0+\frac{g'}{T} , \tag{10}$$

where f' and g' are the derivatives of the low and high-temperature anomalies, respectively. To examine whether f and g vary linearly with ρ_0, we normalize the data as

$$X=\frac{1}{\rho_0T}\frac{d\rho}{dT}-\frac{2A}{\rho_0}=\frac{f'}{\rho_0T}+2B+\frac{g'}{\rho_0T} . \tag{11}$$

If both f and g are proportional to ρ_0, then X should be independent of the concentrations of the alloy samples. Thus a plot of X versus T for all samples should fall on a single curve.

With this background, we now discuss the following properties of our data: residual resistivity per atomic percent impurity, T^2 resistivity component, high-temperature components, and the low-temperature anomaly.

A. Residual resistivity per atomic percent impurity

Figure 2 shows the residual resistivities of our samples as functions of the nominal impurity concentrations c. K and Rb are mutually soluble at all concentrations. In contrast, the maximum solubility of Na in K is only about 2 at. % even with fast cooling. Mg has a maximum solubility of 70 at. % in Li. As shown in the insert of Fig. 2, all of our dilute alloy data for ρ_0 versus c fall along the

straight lines representing the best values of $d\rho_0/dc$ obtained by other people.[19] Figure 2 shows that our moderately concentrated *Li*Mg alloys (filled squares) are also consistent to within experimental uncertainties, with the measurements of Oomi *et al.*[20] (open squares). The values of ρ_0 for all *K*Rb alloys can be fit to the formula $\rho_0 = Ex(1-x)$ with $E \approx 0.114\ \mu\Omega$ m and $x = c/100\%$, as shown by the dashed curve through the *K*Rb data in Fig. 2. Some segregated *K*Na alloy samples with values of ρ_0 much smaller than those expected from their concentrations were made by keeping the samples at room temperature for an extended time. We will discuss the behavior of these samples below.

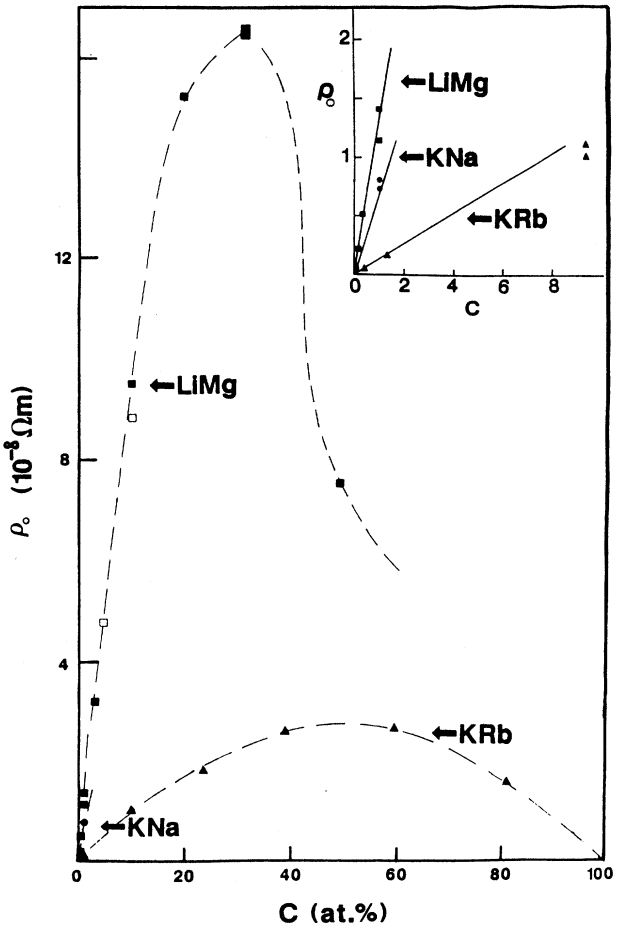

FIG. 2. ρ_0 vs atomic percent impurity concentration c for *K*Rb, *K*Na, and *Li*Mg alloys. The open squares are data of Oomi *et al.* (Ref. 20). In the main figure, the dashed curve through the *K*Rb alloy data is fitted to the formula $\rho_0 = 0.114x(1-x)\ \mu\Omega$ m, with $x = c/100$ at. %; the dashed curve through the *Li*Mg alloy data is merely a guide to the eye. The inset shows detailed data for dilute alloys. The solid lines indicate the best experimental values from Ref. 18 in $10^{-8}\ \Omega$ m/at. %, $d\rho/dc = 0.13$ for *K*Rb, 0.69 for *K*Na, and 1.3 for *Li*Mg.

TABLE I. Estimated and experimental coefficients of the $B\rho_0 T^2$ term in Eqs. (2) and (3).

Sample	B (10^{-6} K^{-2}) B^a	B^b	B^c	B(expt.)
*K*Rb	12.5	$9.3 < B < 15.8$	3.6	11±1
*K*Na				7.0±1
*Li*Mg	3.1			1.5±0.1

[a]Kus and Taylor (Ref. 21).
[b]Mahan and Wang (Ref. 22).
[c](Ref. 18).

B. T^2 resistivity component

We now turn to the temperature-dependent resistivity. Figures 3–6 show plots of $(1/T)(d\rho/dT)$ versus T for *K*Rb, *K*Na, and *Li*Mg alloys, respectively. In the absence of an anomaly, each of these plots would be a horizontal straight line as given by Eq. (4b). This is generally true for very dilute (0.38 at. %) *K*Rb alloys as shown in Fig. 3, for pure K between 0.3 and 1.3 K (inelastic electron-dislocation scattering may be important below 0.3 K, and electron-phonon scattering becomes important above 1 K) as shown in Fig. 4, and for pure Li from 2 K up to higher temperatures than we measured [since θ_D(Li) is much higher] as shown in Fig. 5. As the impurity con-

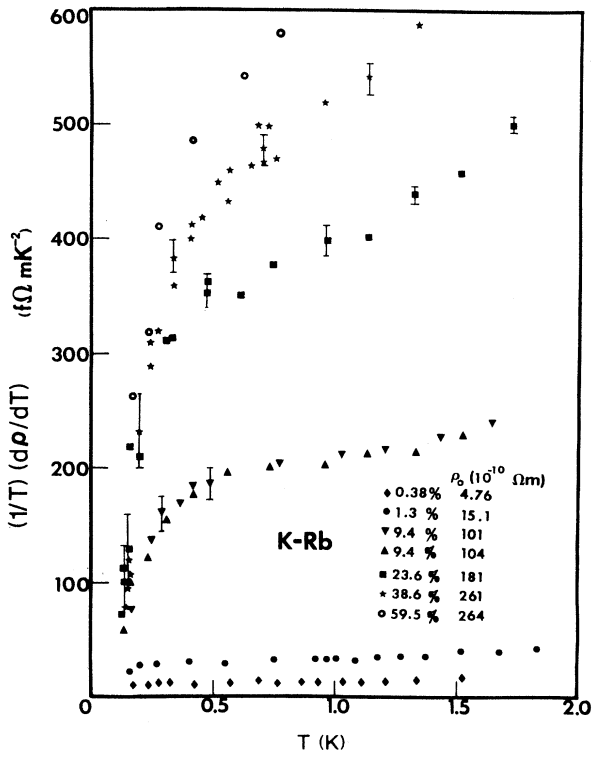

FIG. 3. $(1/T)d\rho/dT$ vs T for all *K*Rb alloy samples.

centrations are increased, however, we see that an anomalous downturn begins to develop at the lowest temperatures in all three alloy systems, and at temperatures above about 1.2 K an upturn, larger than that in pure K, develops for *K*Rb and *K*Na alloys. We will discuss these two new features of Eq. (10) in the next two sections. In this section we concentrate on the T^2 term.

Figure 7 shows the coefficients of the T^2 terms, obtained by fitting the flat parts of the data in Figs. 3–6, for the more dilute (≤ 10 at. %) *K*Rb, *K*Na, and *Li*Mg alloys as a function of the residual resistivity ρ_0. We see that the coefficients are consistent with straight lines for each alloy, as would be expected from Eq. (4b). The values of A found by extrapolating the data back to $\rho_0=0$ agree well with the values measured on the pure host metals.

Table I lists the values of the slopes (i.e., B) of the straight lines, and the values of theoretical calculations for comparison. Our experimental value for B for the *Li*Mg alloys is in good agreement with the value of $(1.6\pm0.2)\times10^{-6}$ K^{-2} obtained by Oomi *et al.*[20] from higher-temperature measurements. The values of B obtained by Kus and Taylor[21] were calculated using the best available pseudopotentials and without invoking the Debye approximation. They also took into account the mass difference between host and impurity ions. Considering the difficulty of these calculations, the agreement with experiment is satisfactory. Very recently Mahan and Wang[22] computed B as a function of the scattering phaseshifts of the electrons by the impurity. For *K*Rb they obtained upper and lower bounds for B that bracket our experimental value (see Table I). They concluded that it would be inappropriate to compare their value of B for cubic *Li*(Mg) with experiment since Li is known to transform to the noncubic 9*R* phase at low temperature.

Recently Hu and Overhauser used a Gaussian potential for Rb in K to estimate the magnitude of B for Rb in K.[18] They found a value (see Table I) only about one-third that of experiment. They concluded that an additional contribution was needed to explain the experimental data, and proposed that this contribution resulted from vertex corrections on elastic impurity scattering. The Gaussian potential is a rather crude approximation for a homovalent impurity compared to the calculation

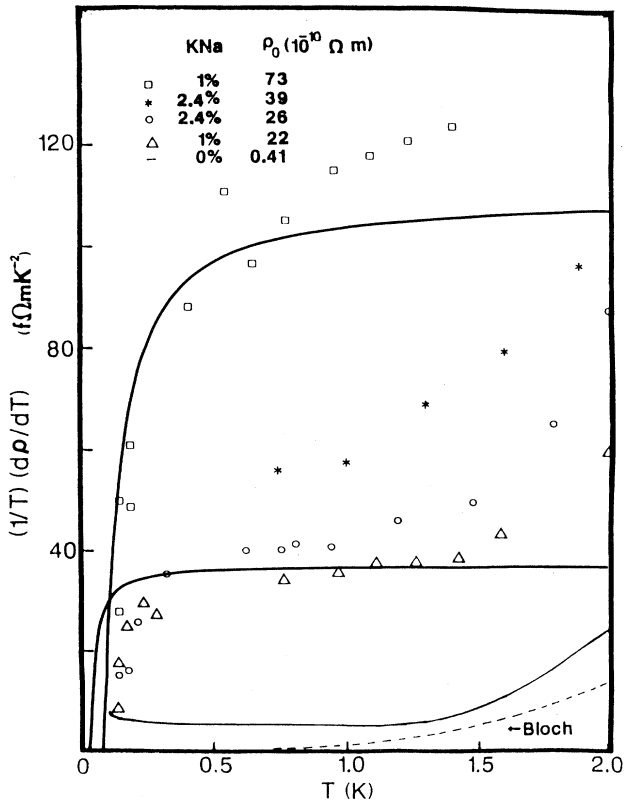

FIG. 4. $(1/T)d\rho/dT$ vs T for all *K*Na alloy samples. The dashed curve is an estimate of the Bloch T^5 term in pure K if phonon drag were absent. The solid curve near the bottom of the graph represents the typical behavior of pure-K samples. The other two solid curves are fits to the data for the 1 at. % samples using the ineffectiveness of electron-phonon scattering model of Kaveh and Wiser (Ref. 17) as discussed later in the text.

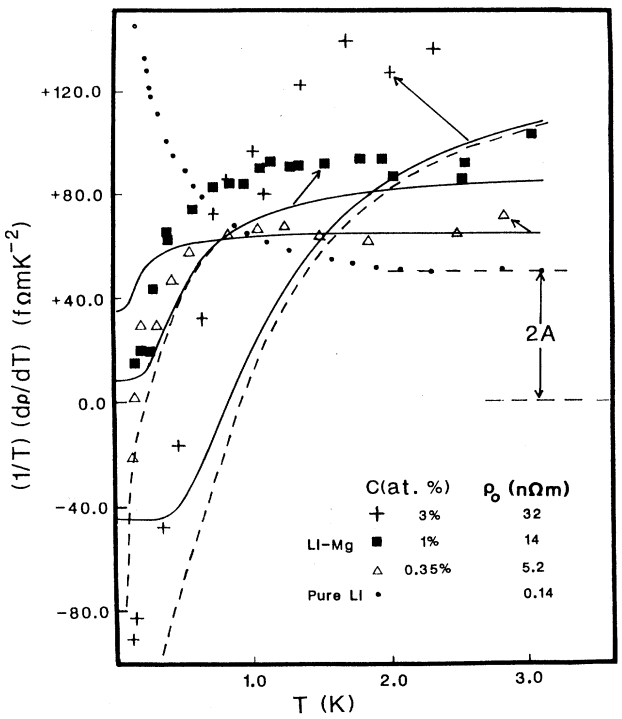

FIG. 5. $(1/T)d\rho/dT$ vs T for dilute *Li*Mg alloys. The solid curves are a fit by the ineffectiveness of electron-phonon scattering model of Kaveh and Wiser (Ref. 17) as discussed later in the text. The arrows indicate the data to which each curve is fit. The dashed curves show the addition to this fit of the electron-electron interaction term, Eq. (18).

by Kus and Taylor, and no independent method was used to determine the value of the adjustable parameter in their estimate. We thus feel that their estimate of B due to inelastic scattering is not definitive. For the present, we will continue to attribute the term proportional to $\rho_0 T^2$ to inelastic impurity scattering, and leave their proposed new contribution to further theoretical analysis.

We noted above, that some of the *K*Na samples were held at room temperature to promote segregation of the Na. Figure 8 shows a detailed plot of $(A+\rho_0 B)$ versus ρ_0 for all the *K*Na data, with the nominal Na concentrations labelled. The fact that the data fall on a single line suggest that the parameter B is not sensitive to segregation in *K*Na alloys. Perhaps the segregated Na atoms are located at grain boundaries, the sample surface, or dislocation cores, where they might not contribute to either ρ_0 or B.

C. High-temperature term

The Debye temperature of Li ($\theta_D = 344$ K) is so high that electron-phonon scattering is unimportant in our current temperature range. As shown in Figs. 5 and 6, for Li-based samples containing up to 10 at. % Mg ($\theta_D \approx 300$ K) no significant high temperature deviations are observed. For the samples containing more than 10 at. % Mg, the data are so dominated by the low-temperature anomaly that it is not possible to reliably isolate any high-temperature deviation.

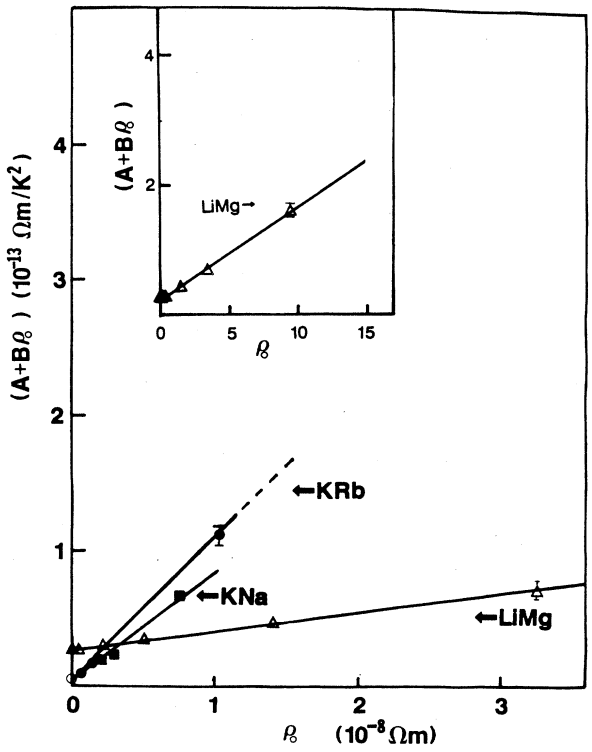

FIG. 7. The coefficients of the T^2 term $A+B\rho_0$ vs ρ_0 for *K*Rb, *K*Na, and *Li*Mg alloy samples. The inset shows data for more concentrated *Li*Mg alloys.

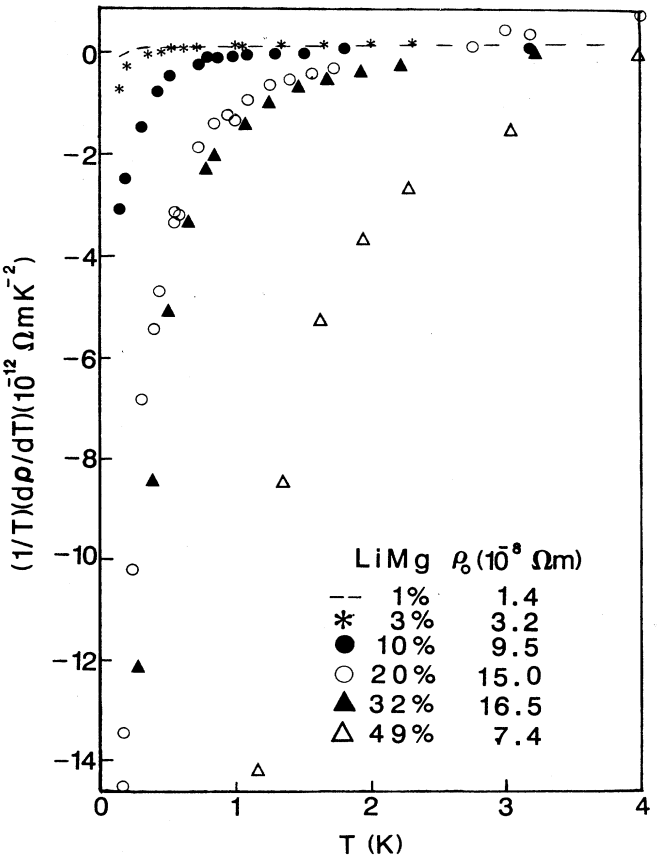

FIG. 6. $(1/T)d\rho/dT$ vs T for all concentrated *Li*Mg alloy samples.

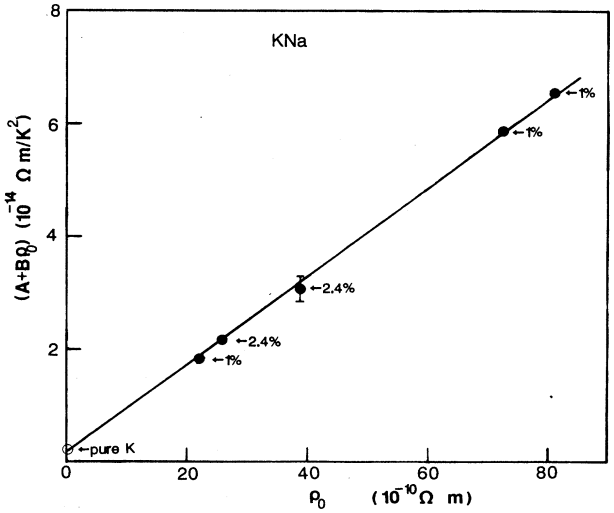

FIG. 8. The coefficients of the T^2 term $A+B\rho_0$ vs ρ_0 for all *K*Na alloy samples. Notice the different ρ_0 values for each Na concentration.

For pure K ($\theta_D \approx 90$ K) electron-phonon scattering can be neglected below 1 K, since phonon-drag greatly reduces the Bloch T^5 component of the N- (normal-) process electron-phonon resistivity and the exponential U- (Umklapp-) process electron-phonon component becomes very small below 1 K.[9,10] When Rb or Na is added to K, however, at high temperatures $d\rho/dT$ begins to increase faster than for pure K, as depicted in Figs. 3 and 4. It seems that the data can be scaled by ρ_0, as illustrated in Fig. 9. We see there that the values of X [see Eq. (11)] for KNa all fall closely around a single curve, as also do the values of KRb alloys up to 23.6% at. %. The deviation from the curve for 38.6 at. % KRb may be due to a large decrease in the Debye temperature due to the high-Rb concentration, as will be discussed below. According to Eq. (11), the different horizontal positions of the two solid curves must be due to a difference between the values of B for KRb and KNa. The fact that such normalization brings the data for each alloy close to a single curve means that f and g are both approximately proportional to ρ_0 for not-too-high concentration alloys.

We first seek the simplest equation which can describe these data. The solid curves in Fig. 9 are fits to $X = -C/T + 2B + HT^3$, where the term $-C/T$ is the best fit to the low-temperature anomaly in dilute alloys, as discussed in Sec. IV D 1 below. The agreement of these fits with the data suggests that

$$g \propto \rho_0 T^n, \quad n \simeq 5 . \tag{12}$$

Due to the experimental uncertainties, n can only be determined to lie within $4 \leq n \leq 6$.

There is a theoretical prediction for a term similar to Eq. (12) by Kagan and Zhernov.[23] In a calculation of coherent electron-impurity scattering, they obtained a term proportional to $\rho_0 T^5$ due to scattering by the deformed phonon spectrum. However, the leading term $\propto \rho_0 T^5$ was predicted to be positive for KRb but negative for KNa; this contradicts our experimental results.

We next consider whether quenching of phonon-drag can completely explain the observed high-temperature behavior by bringing back the T^5 term that phonon drag has removed from pure K.[9,10] Certainly the effects of quenching of phonon drag by impurities can be seen in the thermoelectric ratio data of these alloys.[4] To examine this possibility, we plot the Ekin and Maxfield[24] theoretical calculation of the Bloch T^5 term of pure K in the limit of no phonon drag

$$\rho_{e\text{-}p}^N = 3.5 \times 10^{-16} T^5 \ \Omega\,\mathrm{m/K}^5 ,$$

as a dotted curve in Fig. 4. We see that growth of a T^5 term with increasing ρ_0 is large enough to explain the high-temperature behavior of very dilute KRb and KNa alloys (see Fig. 3). For more concentrated alloys, however, the high-temperature deviations become larger than the Bloch contribution for pure K.

The only simple remaining possibility for explaining the further increase in the magnitude of electron-phonon scattering as the Rb and Na concentrations increase in KRb and KNa are changes in the Debye temperatures from $\theta_D \approx 90$ K for K toward $\theta_D \approx 55$ K as Rb is added to K and toward $\theta_D \approx 150$ K as Na is added to K. We note that changes in θ_D can produce large effects, since the magnitude of the normal Bloch T^5 term is predicted to be proportional to $1/\theta_D^6$, and the Umklapp term is exponential in θ_D—because θ in Eq. (2) is proportional to θ_D.

Wiser[17] has recently shown that the high-temperature term in our KRb data can be well explained by changes in the normal and umklapp electron-phonon terms as θ_D is reduced with increasing Rb concentration. Within the limits of theoretical and experimental uncertainty, he could not eliminate either term from the fit. We thus consider below the effect of including both normal and Umklapp terms on the analysis of the low-temperature anomaly.

Figure 9 shows that the high-temperature behavior in our KNa alloys is very similar to that in the KRb alloys. Unfortunately, Wiser's explanation will not do for the KNa data, since $\theta_D(\mathrm{Na}) > \theta_D(\mathrm{K})$. Although we currently have no explanation for the behavior of the high-temperature KNa data, we speculate that the observed Na segregation may play a role.

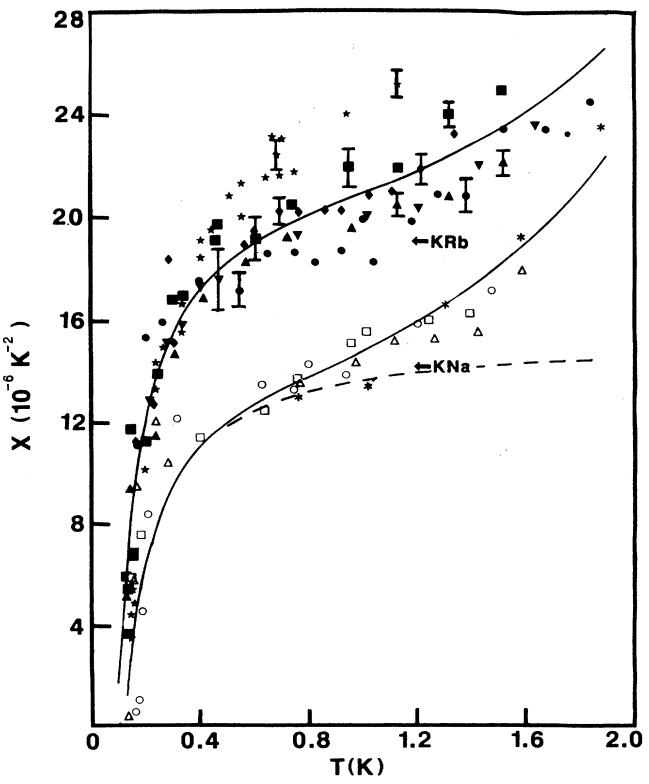

FIG. 9. X vs T for the KRb alloys up to 38.6 at. % Rb and for all the KNa alloys. The solid curves are fits with $X = -C/T + 2B + HT^3$, and the dashed curve is the same fit to the KNa data with the HT^3 term removed. For each sample, the symbol is the same as in Fig. 3 or 4.

D. Low temperature anomaly

1. *Temperature and ρ_0 dependences of the anomaly*

As illustrated in Figs. 3–6, a low-temperature resistivity anomaly develops as ρ_0 increases in all three alloy systems. In particular, Fig. 6 shows how this anomaly in *Li*Mg crosses the zero line (indicating a resistivity minimum) and turns down enormously as ρ_0 is further increased. An interesting feature of the *Li*Mg data in Fig. 5 is the transition from an upward turning anomaly in pure Li to a downward turning anomaly in 0.35 at. % *Li*Mg. As we have already shown for more dilute alloys,[25] this transition appears to be a smooth one and seems to be a detailed display of the competition between two different mechanisms.

As shown in Fig. 9, the low-temperature resistivity anomaly $f(\rho_0, T)$ for all *K*Na and *K*Rb alloys is approximately proportional to ρ_0. The large upturn at low temperatures in dilute *Li*Mg alloy data complicates a similar analysis, and we will demonstrate the linear ρ_0 dependence of dilute *Li*Mg data by a different plot (Fig. 13). To analyze in detail how the low-temperature anomaly varies with T, we first consider the three temperature dependences expected for localization, electron-electron interaction, and the Kondo effect

$$f \propto -T \quad \text{(localization)}, \tag{13}$$

$$f \propto -T^{1/2} \quad \text{(electron interaction)}, \tag{14}$$

$$f \propto -\ln T \quad \text{(Kondo effect)}, \tag{15}$$

for which $(1/T)d\rho/dT$ should be proportional to T^{-1}, $T^{-3/2}$, and T^{-2}, respectively. When we plot $(1/T)d\rho/dT$ as a function of these three powers of T for various samples, we find that all the *K*Rb and *K*Na samples and for dilute *Li*Mg the graphs with the T^{-1} abscissa give slightly better fits than those with $T^{-3/2}$ and that the T^{-2} graphs give the worst fits. Examples of such fits are shown in Fig. 10 for a 23.6 at. % *K*Rb alloy. The dashed, long-dashed, and dotted curves in Fig. 11 illustrated how the three fits to the 23.6 at. % *K*Rb alloy data in Fig. 10 look when converted into a plot of $(1/T)d\rho/dT$ versus T. We note that all three curves fall below the data at sufficiently high temperatures. This is due to the onset of the extra term discussed in the previous section. The solid curves in Figs. 11 and 9 illustrate

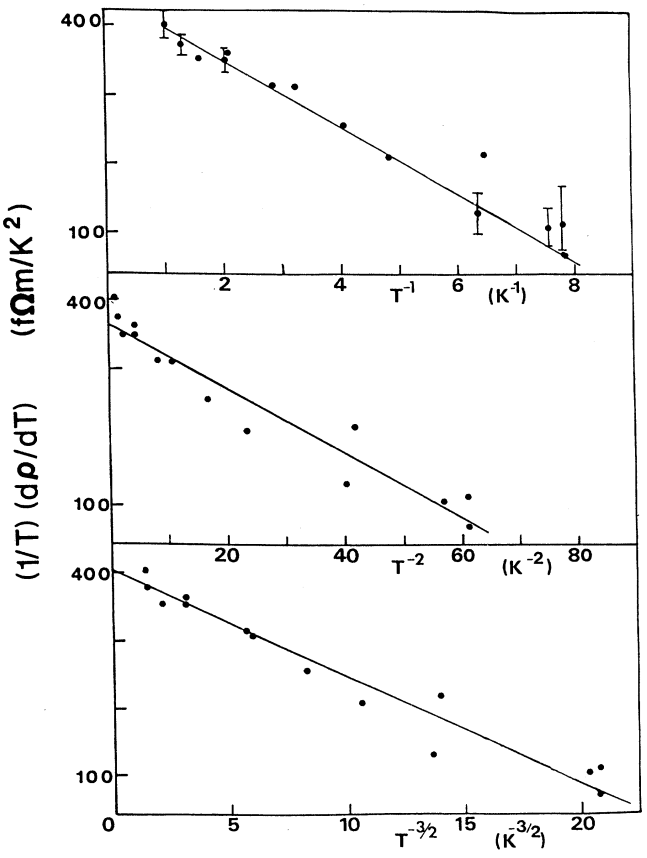

FIG. 10. $(1/T)d\rho/dT$ vs T^{-1}, T^{-2}, and $T^{-3/2}$ for the 23.6 at. % *K*Rb alloy. Note that the data above 1 K are not plotted.

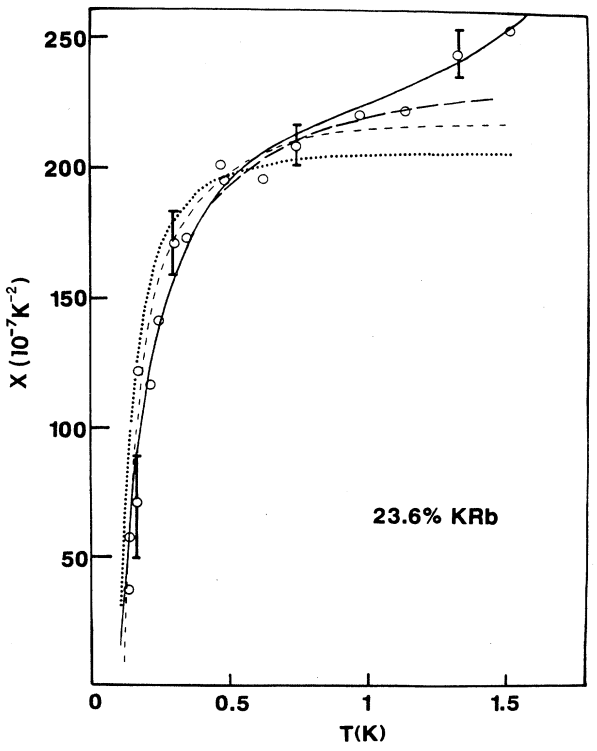

FIG. 11. X vs T for 23.6 at. % *K*Rb. The long-dashed, dashed, and dotted curves are fits to Eqs. (13), (14), and (15), respectively. The solid curve is fit to Eq. (16) along with an additional T^5 term.

how a resistivity term linear in T (long-dashed curve in Fig. 11) along with an additional T^5 term fit the 23.6 at. % *K*Rb data. A similar fit for the *K*Na alloys is illustrated by the solid line in Fig. 9. We conclude that our data can be fit with a low-temperature anomaly that is linear in both T and ρ_0, plus a high-temperature anomaly that varies approximately as T^5. This is the simplest fit to our data.

We cannot, however, rule out more complex fits. For example, if we choose to include *two* high-temperature terms (T^5 plus an exponential), we can fit the entire range of data for each alloy—to within experimental uncertainty—using each of the three forms given in Eqs. (13)–(15). In the absence of detailed knowledge of the magnitudes of these two high-temperature terms, we choose to parametrize our results using the low-temperture form which, by itself, fits the data over the widest temperature range. This is $f \propto -T$. Combining this best fit with the fact that $f \propto \rho_0$, we offer an approximate empirical equation for our data at low temperature:

$$\rho = \rho_0 + AT^2 + B\rho_0 T^2 - C\rho_0 T \ . \tag{16}$$

If Eq. (16) is applicable, then plots of $d\rho/dT$ versus T for the data should give straight lines which do not pass through the origin. The intercept with the abscissa should give the coefficient $C\rho_0$. Such plots are given in Figs. 12 and 13. We see that for *K*Rb, *K*Na, and dilute *Li*Mg the data appear to be consistent with straight lines, corresponding to a resistivity anomaly of the form

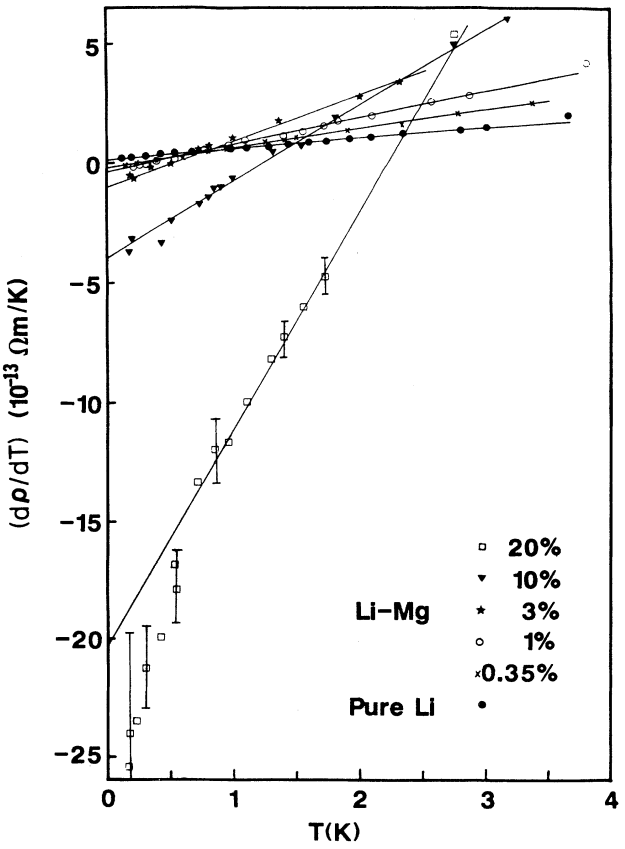

FIG. 13. $d\rho/dT$ vs T for *Li*Mg alloys.

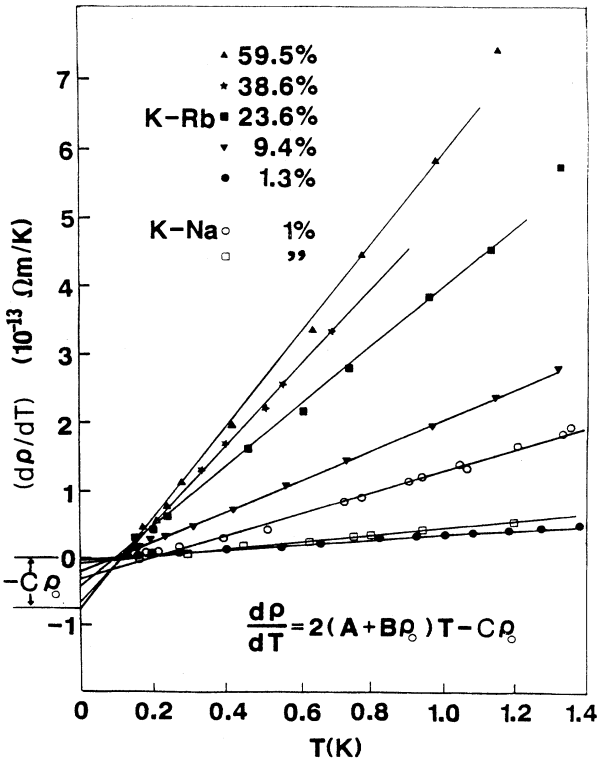

FIG. 12. $d\rho/dT$ vs T for *K*Rb and *K*Na alloys.

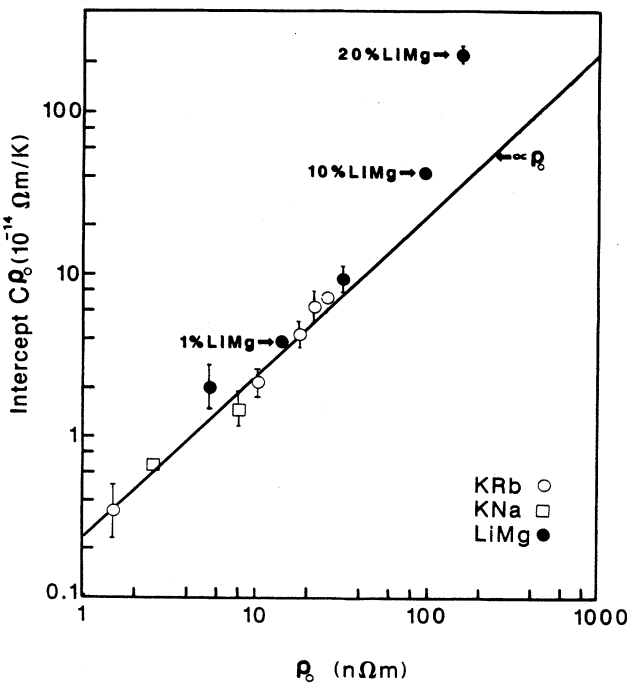

FIG. 14. Log-log plot of the intercepts of the data in Figs. 12 and 13 vs ρ_0.

$f \propto \rho_0 T$. Figure 13 also shows that the data begin to deviate from a straight line for *Li*Mg alloys with Mg concentration higher than 10% ($\rho_0 > 10^{-7}$ Ω m). Figure 14 shows the coefficient $C\rho_0$ versus ρ_0. We see that for $\rho_0 < 10^{-7}$ Ω m, the data for all three alloys are consistent, to within the uncertainties, with a linear dependence upon ρ_0 and a *single value* for the coefficient C. On the other hand, when the *Li*Mg alloy data are extended to $\rho_0 > 10^{-7}$ Ω m, the data increase faster than ρ_0. Therefore, both the temperature and the residual resistivity dependences of the low-temperature resistivity anomaly of *Li*Mg alloys seem to depart from $f \propto \rho_0 T$ for $\rho_0 > 10^{-7}$ Ω m. To examine the T dependence of the anomaly for high concentration *Li*Mg alloys, we plot the data as $(1/T)d\rho/dT$ versus $T^{-3/2}$ and T^{-1} in Fig. 15 to compare the data with the predicted interaction and localization forms, respectively. This shows that the $T^{-3/2}$ form associated with interactions becomes a better fit as the Mg concentration increases. Figure 16 (to be discussed in more detail in Sec. IV D 2) is a plot of the coefficients of the $T^{-3/2}$ term in $(1/T)d\rho/dT$ versus ρ_0 for all of our samples (the data for $\rho_0 < 10^{-7}$ Ω m are *forced* to this form). We see how the data change from a ρ_0 dependence (dashed line) to $\rho_0^{5/2}$ (solid line) as ρ_0 increases.

To summarize the experimental data, we rewrite the best-fit form for the low-temperature resistivity anomaly as

$$f = -C\rho_0 T \quad \text{for } \rho_0 < 10^{-7}\ \Omega\,\text{m}\ , \tag{17}$$

$$f = -D\rho_0^{5/2} T^{1/2} \quad \text{for } \rho_0 > 10^{-7}\ \Omega\,\text{m}\ , \tag{18}$$

where, due to the uncertainties, the power of the temperature dependence in Eq. (17) can only be determined to lie between $\frac{1}{2}$ and 2.

For *Li*Mg samples containing 32 at. % or more Mg, we found that heat treatment begins to affect the resistivity anomaly, although it has little or no effect on the residual resistivity. The different 32 at. % data points in Fig. 16 correspond to different annealing treatments. Their differences suggest that an inhomogeneous impurity distribution somehow affects the behavior of the anomaly. Presumably the unexpected high value of the data point for the *Li*(49 at. % Mg) sample is also associated with an inhomogeneous microstructure. The reason for these behaviors is not yet clear.

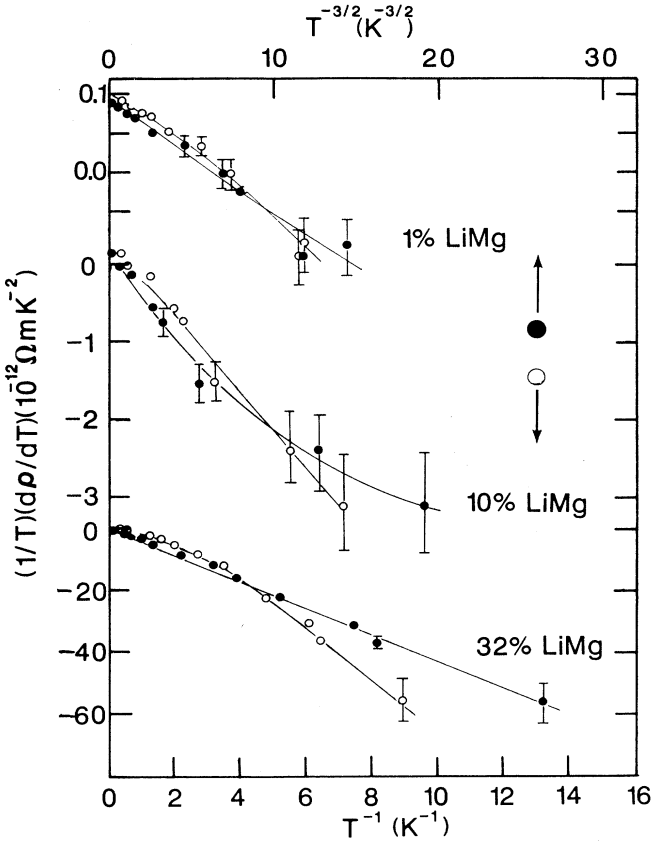

FIG. 15. $(1/T)d\rho/dT$ vs T^{-1} and $T^{-3/2}$ for 1 at. %, 10 at. %, and 32 at. % *Li*Mg alloys. The curves are only guides to the eye.

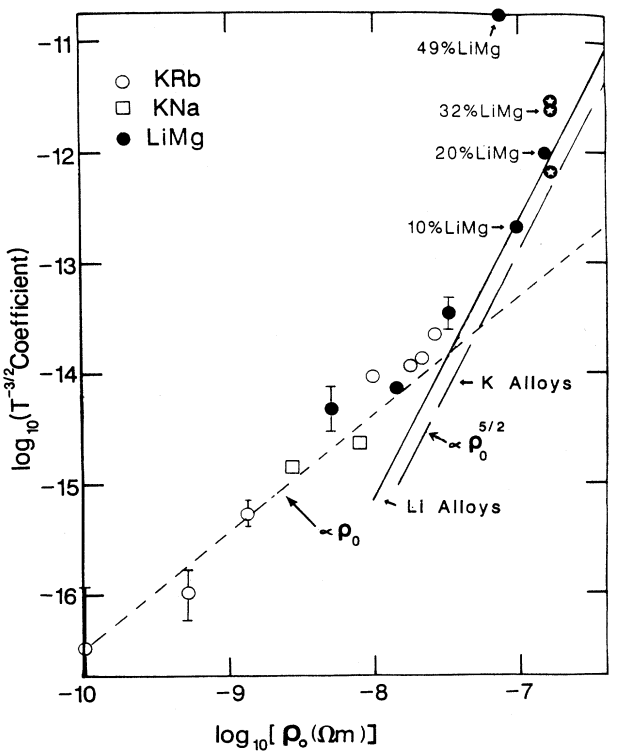

FIG. 16. Log-log plot of the coefficients of the corresponding $T^{-3/2}$ term in $(1/T)d\rho/dT$ vs ρ_0 for all alloy samples. The dashed line is a ρ_0 dependence. The solid and long-dashed lines are $\rho_0^{5/2}$ dependences for Li and K based alloys, respectively, from electron-electron interaction theory.

2. *Comparison with theoretical models*

We have just seen that the low-temperature anomaly contributes a negative resistivity term at low temperatures, the magnitude of which grows with increasing ρ_0. In the following we compare the data with models which might explain such behavior.

The Kondo effect. To test if the anomaly is caused by the Kondo effect, we measured the magnetic field dependence of the anomaly, as described elsewhere.[1] Both the *K*Rb (9.7 at. %) and *Li*Mg (1 at. %) alloy data show no magnetic field dependence up to 0.2 T, the maximum field available. A simple estimate predicts that a field of 0.2 T should have essentially eliminated the Kondo anomaly in the vicinity of 0.1 K. Therefore, the Kondo effect seems to be ruled out. Moreover, as we describe in Ref. 4, we find no Kondo-type anomalies in the thermoelectric properties.

Two-level system (TLS). The anomaly for a TLS is expected to be independent of magnetic field. Moreover, the extra parameter T_0 in the TLS logarithmic temperature-dependent form permits an improvement in the logarithmic fit to the $\rho(T)$ of our alloy data. However, our samples are crystalline, and it is difficult to see—especially for *K*Rb where the host and impurity atoms have the same charge and close to the same size—how isolated impurities, or the nearby K atoms, could be free to tunnel between two alternative positions. Since one would expect tunneling states to be sensitive to different atom sizes and different host and impurity charges, it is also difficult to see how a tunneling model could lead to the universality of behavior we find for all three alloy systems studied.

The effect of electron-phason interactions. As indicated above, Hu and Overhauser[18] have proposed CDW-based effects as an explanation for our data. However, when we examine the fit of their model to our data,[18] we find that they predict too rapid a falloff of $(1/T)(d\rho/dT)$ with increasing temperature for temperatures between 1 and 0.2 K, and what appears to be a limiting minimum value at about 0.2 K. Our data, in contrast, are still rapidly decreasing below 0.2 K. Clearly this interesting model needs further investigation, including an analysis of whether it predicts similar behavior for *Li*Mg alloys.

Ineffectivness of electron-phonon scattering. We noted above that Kaveh and Wiser[17] were able to fit our *K*Rb data down to 0.1 K assuming a phonon cut-off wave vector $q_{\min}=\pi/l$ in Taylor's expression for inelastic electron-impurity scattering. A useful parameter for comparing the Kaveh-Wiser model with the data is the "crossover temperature" T_0 at which $(1/T)d\rho/dT=2A$. For the above choice of $q_{\min}$, one obtains theoretically that $T_0\approx(0.8)\theta_D/lk_F$, where k_F is the Fermi wave vector. For this model we expect that $T_0\propto\rho_0$ since $\rho_0\propto 1/l$. In contrast, the data for the *K*Rb and *K*Na alloys in Fig. 9 show that the experimental values of T_0 do not vary significantly compared with the factor-of-10 range exhibited by ρ_0 in this figure. However, for the *Li*Mg alloys where $A=25$ fΩ m/K^2, the data in Fig. 5 show a more significant dependence of T_0 upon ρ_0, especially for the 3 at. % sample compared with the 0.35 and 1 at. % samples.

In Fig. 4 the upper two solid curves represent the fits of the Kaveh-Wiser model to the two 1 at. % *K*Na alloys with $A=2.4$ fΩ m/K^2, $B=7.3\times10^{-6}$ K^{-2}, and $\theta_D=90$ K. As expected, the curves show that T_0 increases with increasing ρ_0. Although these fits are in semiquantitative agreement with the data, the theoretical values of T_0 are too small. For the *Li*Mg alloys, if B is chosen to be 1.5×10^{-6} K^{-2} which is our value from Table I and θ_D is $=344$ K, the Kaveh-Wiser model (solid curves in Fig. 5) produces only qualitative fits to the *Li*Mg data of Fig. 5, particularly for the 3 at. % alloy. The dashed curves show the effect of adding the electron-electron interaction term [Eq. (18)] to the Kaveh-Wiser fit for the 1 and 3 at. % samples. These fits can be improved somewhat by raising B to 2.4×10^{-6} K^{-2}. However, this value is unrealistically large since B is constrained by the data of Oomi *et al.*[20] who determined B from data taken up to 8 K where the correction to $\rho(T)$ due to the Kaveh and Wiser model is smaller than for temperatures below 2 K. Thus for the Kaveh-Wiser model the ρ_0 dependence of T_0 is too large, giving a value of T_0 that is too small for the lower-ρ_0 alloys such as *K*Na in Fig. 4 and is too large for the highest-ρ_0 alloy in Fig. 5, the 3 at. % *Li*Mg sample. We conclude that the Pippard ineffectiveness model in its current form provides a qualitative, but not quantative, description of our results.

Localization and interaction. To test the applicability of these two models, we compare our data with the theoretical calculations given by Lee and Ramakrishnan.[3] As discussed above, if we assume that the nonanomalous contribution to $\rho(T)$ [i.e., Eq. (3)] is dominated by inelastic electron-impurity scattering, then for our values of ρ_0 the theory predicts that the interaction term should predominate, and $(1/T)d\rho/dT$ should vary as $T^{-3/2}\rho_0^{5/2}$ as given by Eq. (8) and found empirically in Eq. (18). Figure 15 shows that the $T^{-3/2}$ dependence of Eq. (18) is consistent with *Li*Mg data having $\rho_0>10^{-7}$ Ω m. To compare the predicted magnitude of interaction effects with the experimental data, the coefficients of the $T^{-3/2}$ term have been estimated for our *K*Rb, *K*Na, and *Li*Mg alloys from plots such as the one shown in Fig. 10.

These coefficients are plotted versus ρ_0 on a log-log plot in Fig. 16. The solid line and the broken solid line in Fig. 16 are the predicted behavior for interaction effects in Li- and K-based alloys, respectively. For small values of ρ_0 the data in Fig. 16 are consistent with a linear dependence on ρ_0, as indicated by the dashed line, and the data fall well above the solid and broken lines. This shows that these quantum effects are too small to account for the anomaly in these samples. As ρ_0 increases above about 10^{-7} Ω m, however, the data break away from the dashed line, and appear to approach the solid line.

V. SUMMARY AND CONCLUSIONS

(1) The residual resistivities of our *K*Rb, *K*Na, and *Li*Mg alloys are consistent with those obtained by previous investigators in the regions of overlap.

(2) The T^2 resistivity components we observe are con-

sistent with a simple sum of electron-electron scattering and inelastic impurity scattering. The magnitude of the inelastic impurity scattering terms are compatible with theoretical predictions.

(3) Electron-phonon scattering becomes evident in *K*Rb and *K*Na alloys above about 1 K. In the dilute alloys, as in pure K, the exponential term due to Umklapp electron-phonon scattering seems to remain dominant. As the impurity concentration increases, however, the T^5 term associated with normal electron-phonon appears to grow, first probably due to partial quenching of phonon drag, and later, at least in *K*Rb, due to decreasing of the Debye temperature θ_D of the alloy which also strongly affects the Umklapp term. As Wiser[17] has recently shown, the high-temperature behavior of the *K*Rb data can be well explained by changes in θ_D, but a similar explanation fails for the very similar looking data for *K*Na. Due to the high Debye temperature of Li, none of the *Li*Mg alloys shows any evidence of electron-phonon scattering up to 4 K, the highest temperature measured.

(4) We have discovered a new low-temperature anomaly in the electrical resistivities of *K*Rb, *K*Na, and *Li*Mg alloys. All of the available data are consistent with an anomaly which is the same for all three alloys at any given value of the residual resistivity ρ_0. For $\rho_0 \leq 10^{-7}$ Ω m, the anomaly can be parametrized by the equation $\rho(T) = -C\rho_0 T$. This anomaly is not due to the Kondo effect, or to localization and interaction effects. Further theoretical work needs to be done to confirm the applicability and to understand better the magnitude of the Kaveh and Wiser model for ineffectiveness of electron-phonon scattering or of the Hu and Overhauser CDW-based model. For $\rho_0 \geq 10^{-7}$ Ω m, the data shift to a different form, which can be parametrized by $\rho(T) = -D\rho_0^{5/2}T^{1/2}$. Both this form and the magnitude of the term in this regime are consistent with expectation for electron-electron interactions in a disordered alloy. For very-high-concentration *Li*Mg alloys the details of the microscopic structure of the samples seem to affect the anomaly. The reasons for this behavior are not yet understood.

ACKNOWLEDGMENTS

This paper is based in part upon the Ph.D. thesis of J. Zhao. The work was supported in part by the National Science Foundation (NSF) Division of Materials Research through the Low Temperature Physics Program Grants No. DMR-83-03206, No. DMR-83-05289, and No. DMR-87-00900.

*Present address: EMCORE Corporation, 35 Elizabeth Ave., Somerset, NJ 08873.

†Present address: Xerox Corporation, Joseph C. Wilson Center for Technology (0114-24D), W114, 800 Phillips Road, Webster, NY 14580.

‡Present address: Honeywell, Inc. (S11/2920), 600 Second Street N., Hopkins, MN 55343.

§Present address: Low Temperature Laboratory, Helsinki University of Technology, SF-02150 Espoo 15, Finland.

**Present address: Department of Physics, Tokyo Metropolitan University, 2-1-1 Fukazawa, Setagaya-ku, Tokyo 158, Japan.

[1]J. Bass, L. Hearle, W. P. Pratt, Jr., Y. J. Qian, P. A. Schroeder, S. Yin, Z.-Z. Yu, and J. Zhao, Phys. Rev. Lett. **56**, 957 (1986).

[2]J. Kondo, Prog. Theor. Phys. **32**, 37 (1964).

[3]P. A. Lee and T. V. Ramakrishnan, Rev. Mod. Phys. **57**, 287 (1985).

[4]J. Zhao, Z.-Z. Yi, H. Sato, W. P. Pratt, Jr., P. A. Schroeder, and J. Bass (unpublished).

[5]D. L. Edmunds, W. P. Pratt, Jr., and J. A. Rowlands, Rev. Sci. Instrum. **51**, 1517 (1980).

[6]J. M. Ziman, *Electrons and Phonons* (Oxford University Press, London, 1960).

[7]S. Koshino, Prog. Theor. Phys. **24**, 484 (1963); **24**, 1049 (1960); P. L. Taylor, Phys. Rev. **135**, A1333 (1964).

[8]L. Landau and I. Pomeranchuk, J. Phys. Sowjetunion **10**, 649 (1936).

[9]H. van Kempen, J. S. Lass, J. H. J. M. Ribot, and P. Wyder, Phys. Rev. Lett. **37**, 1574 (1976).

[10]J. A. Rowlands, C. Duvvury, and S. B. Woods, Phys. Rev. Lett. **40**, 1201 (1978).

[11]M. Kaveh and N. Wiser, Phys. Rev. Lett. **29**, 1374 (1972).

[12]Z.-Z. Yu, M. Haerle, J. W. Zwart, W. P. Pratt, Jr., P. A. Schroeder, and J. Bass, Phys. Lett. **97A**, 61 (1983).

[13]G. Krill, Solid State Commun. **9**, 1065 (1971).

[14]M. L. Haerle, W. P. Pratt, Jr., and P. A. Schroeder, J. Low. Temp. Phys. **62**, 397 (1986).

[15]R. W. Cochrane and J. O. Strom-Olsen, Phys. Rev. B **29**, 1088 (1984); R. Harris and J. O. Strom-Olsen, in *Glassy Metals II,* edited by H. Beck and H. Güntherodt (Springer-Verlag, New York, 1983), p. 325.

[16]A. W. Overhauser, Adv. Phys. **37**, 343 (1978).

[17]M. Kaveh and N. Wiser, Phys. Rev. B **36**, 6339 (1987); N. Wiser, J. Phys. F **18**, 457 (1988).

[18]S. P. Hu and A. W. Overhauser, Bull. Am. Phys. Soc. **30**, 261 (1985); S. Hu, Ph.D. thesis, Purdue University, 1987.

[19]J. Bass, *Landolt-Börnstein, Metals: Electronic Transport Phenomena,* edited by K.-H. Hellwege and J. L. Olsen (Springer-Verlag, Berlin, 1982), New Series, Gp. III, Vol. 15a.

[20]G. Oomi, M. A. K. Mohamed, and S. B. Woods, J. Phys. F **15**, 1331 (1985).

[21]F. W. Kus and D. W. Taylor, J. Phys. F **10**, 1495 (1980).

[22]G. D. Mahan and Zongcheng Wang, Phys. Rev. **39**, 4926 (1989).

[23]Y. Kagan and A. P. Zhernov, Zh. Eksp. Teor. Fiz. [Sov. Phys—JETP **23**, 737 (1966)].

[24]J. W. Ekin and B. W. Maxfield, Phys. Rev. B **4**, 4215 (1971).

[25]J. Zhao, J. Bass, W. P. Pratt, Jr., and P. A. Schroeder, J. Phys. F **16**, L271 (1986).